Effects of Collision and Vibrational Energy on the Reaction of $CH_3CHO^+(v)$ with C_2D_4†

Ho-Tae Kim, Jianbo Liu, and Scott L. Anderson*

Department of Chemistry, University of Utah, 315 S. 1400 E. RM Dock, Salt Lake City, Utah 84112-0850

Received: January 23, 2002; In Final Form: March 19, 2002

The reaction of acetaldehyde cations with ethene has been studied as a function of collision energy and acetaldehyde vibrational state. REMPI through different vibrational levels of the $\tilde{B}$ electronic state is used to produce CH_3CHO^+ with controlled excitation in different vibrational modes. Reactions are studied in a guided ion beam instrument, including measurements of product ion recoil velocity distributions. In addition, we calculated the structures and energetics of 13 different complexes that potentially could serve as intermediates to reaction. Three reactions are observed. Hydrogen atom transfer (HT) dominates at low collision energies and is suppressed by collision energy and, to a lesser extent, vibration. The HT reaction is clearly direct at high collision energies but appears to be mediated by a reactant-like precursor complex at low energies. The most energetically favorable product channel corresponds to elimination of CH_3 from an intermediate complex. Nonetheless, this channel accounts for only ~0.5% of the total product signal. The cross section for endoergic charge transfer (CT) is strongly enhanced by collision energy in the threshold region. Over a wide range of collision and vibrational energy, CH_3CHO^+ vibrational excitation enhances CT, but only 18% as much as for the equivalent amount of collision energy. This effect is interpreted in terms of competition between the CT and other product channels. The expected proton-transfer channel is not observed, an absence also attributed to competition.

I. Introduction

Reactions of polyatomic ions and molecules are often mediated by collision complexes that allow time for rearrangements that cannot occur in direct scattering. Several types of complexes are possible. Nearly any ion−molecule system will have reactant-like electrostatic complexes with well depths of a few tenths of an electronvolt with respect to reactants. Such complexes can be very important at low collision energies, where they can mediate reorientation of reactants and help trap reactants into more stable complexes where reactions are possible. Hydrogen-bonded complexes are more strongly bound, providing time for more complex rearrangements and directly mediating H or H^+ transfer reactions. In systems where one or both reactant is unsaturated, covalently bound complexes also exist. If these covalent complexes are accessible, long collision times are possible, allowing complicated reactions with multiple bonds broken and formed.

The $CH_3CHO^+ + C_2H_4$ system has all three types of complexes, with binding energies ranging from ~0.03 to 3 eV. The data provide evidence that the most strongly bound complexes are unimportant in the reaction, whereas the electrostatic and hydrogen-bonded geometries play an important role at low collision energies. Even in the absence of any special vibrational mode effects on reaction, comparing the effects of reactant vibration and collision energy provides insight into the reaction mechanism. Changes in collision energy also change collision velocity and angular momentum, affecting both the probability of complex formation and the branching in complex decay. Vibration, on the other hand, simply increases the vibrational energy of complexes that form. By comparing collision energy and vibrational effects, it is possible to separate partially the influences of complex formation, lifetime, and decay branching. In addition to complex-mediated mechanisms, which usually dominate at low collision energies, most polyatomic ion−molecule reactions make a gradual transition to direct dynamics with increasing energy. For the CH_3CHO^+−C_2H_4 system, there is an important direct mechanism even at low collision energies, which is the regime where most collisions form at least short-lived complexes. Vibration and collision energy have different effects on the branching between direct and complex mechanisms and provide insight into the factors that control this branching.

One interesting feature of the acetaldehyde−ethene system is that there are two pairs of product channels that differ only in which fragment carries the charge. One pair is $CH_3CHO + C_2H_4^+$ versus $CH_3CHO^+ + C_2H_4$ (i.e., charge transfer (CT) vs "separation back to reactants"). The other is $CH_3CO + C_2H_5^+$ versus $CH_3CO^+ + C_2H_5$ (i.e., proton transfer (PT) vs hydrogen atom transfer (HT)). In the CT versus "back to reactants" pair, CT has a substantial cross section despite being endoergic by 0.28 eV. In the PT versus HT pair, PT is not observed at all despite being endoergic by only 0.03 eV. The collision energy and vibrational effects can be understood in terms of the competition between the two product channels.

II. Experiment and Calculations

The guided ion beam (GIB) tandem mass spectrometer used in this study has been described previously,[1] along with operation, calibration, and data analysis procedures. Vibrationally state-selected beams of CH_3CHO^+ were prepared by resonance-enhanced multiphoton ionization (REMPI) of a pulsed, seeded supersonic beam of CH_3CHO. The gas mixture for the beam was prepared by vaporizing liquid acetaldehyde (Fisher Scientific, 99.5%) at about 30 °C and entraining the vapor in 200 psi of helium carrier (Matheson 99.9%). The

† Part of the special issue "Jack Beauchamp Festschrift".

* Corresponding author. E-mail: anderson@chemistry.utah.edu.

10.1021/jp0202284 CCC: $22.00
Published on Web 04/26/2002

TABLE 1: Summarized Results of REMPI−PES Experiment with CH_3CHO

intermediate $\tilde{B}$ state level	ion states observed in PES	average ion vibrational energy (eV)
origin	vibrationless **(**100%**)**	0
10^1	10^1 **(**100%**)**	0.045
9^1	9^1(47%); $9^1 10^1$(26%); 8^1(27%)	0.13
6^1 or 7^1	$6^1 10^1$(29%); $14^1 9^1$(37%); $6^1 15^1$(34%)	0.195
5^1	$5^1 10^1$ **(**90%**)**; 5^1 (10%)	0.22
3^1	$3^1 10^2$ **(**80%**)**; $3^1 15^2$ (15%); 3^1 (5%)	0.44

mixture was expanded through a pulsed valve, collimated by a skimmer, and then introduced into the ionization region.

Preparation of state-selected CH_3CHO^+ cations by REMPI through the acetaldehyde $\tilde{B}$ state has been discussed in detail elsewhere.[2] The vibrational states, or mixtures of states, resulting from each REMPI transition are listed in Table 1. The origin, 10_0^1, 5_0^1, and 3_0^1 transitions generate ions with >80% in a single vibrational state, with the remaining ions also having excitation of the dominant mode. The two other transitions produce cations with no dominant state but with one mode or combinations thereof dominating the distribution. For the present system, there are no mode-specific effects; therefore, we will not emphasize the nature of the different reactant states. We note only that ν_3 is the aldehyde CH stretch (i.e., the stretch of the bond being broken in the hydrogen-transfer reaction). Note that CH_3CHO^+ has low-lying isomers; however, the vibrational energies selected are all well below the isomerization activation barriers,[3−8] thus the parent ion is stable.

The pulse of ions resulting from REMPI is injected into a quadrupole ion guide that focuses the ions through an exit aperture. A set of ion lenses then injects the ions through a gate electrode set and into the first of a pair of 8-pole ion guides where reactions are studied. A combination of the focusing properties of the quadrupole guide and time-of-flight (TOF) gating is used to narrow the energy spread of the beam prior to injection into the reaction region. The first 8-pole guide passes the ions through a scattering cell containing C_2D_4 vapor (Cambridge Isotope Laboratories, >98 atom % D) at 4.5×10^{-5} Torr that is controlled by a leak valve and measured with a Baratron capacitance manometer. All ion intensity measurements are made both with the C_2D_4 flow routed into the scattering cell and with the identical flow routed into the vacuum chamber that houses the scattering cell. By subtracting intensities with the scattering cell filled and "empty", we account for background sources including noise, reactions occurring outside the cell, and the presence of fragment ions in the reactant beam (see below). Product ions and unreacted CH_3CHO^+ are collected by the ion guide and then pass into a second, longer guide where TOF analysis can be used to measure both primary and product ion velocity distributions. The ions are finally mass analyzed by a quadrupole mass spectrometer and counted.

Nascent CH_3CHO^+ produced by 2 + 1 REMPI can absorb an additional photon and fragment to $HCO^+ + CH_3$ or $CH_3CO^+ + H$. The HCO^+ fragments are completely eliminated by time-of-flight (TOF) gating prior to injection into the reaction guide, and CH_3CO^+ is controlled by defocusing the laser.[2] The percentage of CH_3CO^+ in the CH_3CHO^+ beam is kept below 2%. There are two potential problems. The fragment ions might react, affecting the apparent cross sections at both the CH_3CO^+ and product masses. Fortunately, all reactions of the very stable CH_3CO^+ with C_2D_4 are endoergic by at least 2.1 eV (i.e., more than the maximum collision energy in our experiment). CH_3CO^+ is also the product ion in the hydrogen atom transfer (HT) reaction of CH_3CHO^+ with ethene, but at a <2% contamination level, the contribution of the fragment ion in the reactant beam is adequately removed by the subtraction procedure described above. The only problem is with the HT channel for CH_3CHO^+ produced by pumping through the 3_0^1 transition, where the parent intensity is very low and it is impractical to keep the CH_3CO^+ contamination below 2%. To eliminate any possible problems with subtraction of the CH_3CO^+ signal from fragments in the beam, a set of experiments was performed with a modified source arrangement. The quadrupole ion guide was replaced by a conventional quadrupole mass filter, thus completely removing the CH_3CO^+ background. The mass filter source was not used for all experiments because the translational energy spread of the ion beam (<0.2 eV fwhm) is badly broadened (~0.5 eV) by interaction with fringe fields in the mass filter. With the exception of energy resolution, the two sets of data are identical within the scatter of the data.

To aid in reaction coordinate interpretation and to get energetic information, ab initio calculations were performed using MP2 and B3LYP theories with 6-31G* and 6-311++G** basis sets, respectively, using Gaussian 98.[9] Geometries were optimized by calculating both gradients and Hessians at each step, and the geometries and relative stabilities at the MP2 and B3LYP levels are consistent. MP2 and B3LYP zero-point energies were scaled by 0.9646 and 0.9804, respectively.[10] Reactant, product, and complex energies were also calculated at the G3 level of theory, and single point energies were calculated at the QCISD(T)/6-31G* level for all B3LYP/6-311++G** stationary points. Figure 1 summarizes the important energetics, with values taken from the literature,[11,12] when available, or from the G3 calculations. RRKM rate calculations were done with the program of Zhu and Hase[13] using its direct state count algorithm, scaled frequencies from our B3LYP/6-311++G** calculations,[10] and energetics from the literature (when available)[11] or from our calculations.

III. Results

Integral Cross Sections. The integral cross sections for the reaction of ground-state CH_3CHO^+ with C_2D_4 are shown in Figure 2 over the collision energy (E_{col}) range from 0.1 to 2.0 eV. Product ions are observed at m/z 32, 43, and 61 corresponding to $C_2D_4^+$, CH_3CO^+, and $C_3D_4HO^+$, respectively. The energetics of the three observed product channels are as follows:[11]

$$CH_3CHO^+ + C_2D_4 \rightarrow C_2D_4^+ + CH_3CHO$$
charge transfer (CT) $\Delta H = 0.28$ eV
$$\rightarrow CH_3CO^+ + C_2D_4H$$
hydrogen transfer (HT) $\Delta H = -1.08$ eV
$$\rightarrow CD_2CDCHOD^+ + CH_3$$
methyl elimination (ME_1) $\Delta H = -0.91$ eV
$$\rightarrow C_2D_4HCO^+ + CH_3$$
methyl elimination (ME_2) $\Delta H = -1.43$ eV

The experiments used the $CH_3CHO^+ + C_2D_4$ isotope combination to allow the observation of atom scrambling in conjunction with the reactions. For this system, however, only a single mass is observed for each product ion, indicating that H/D exchange is insignificant. Our experiments can distinguish

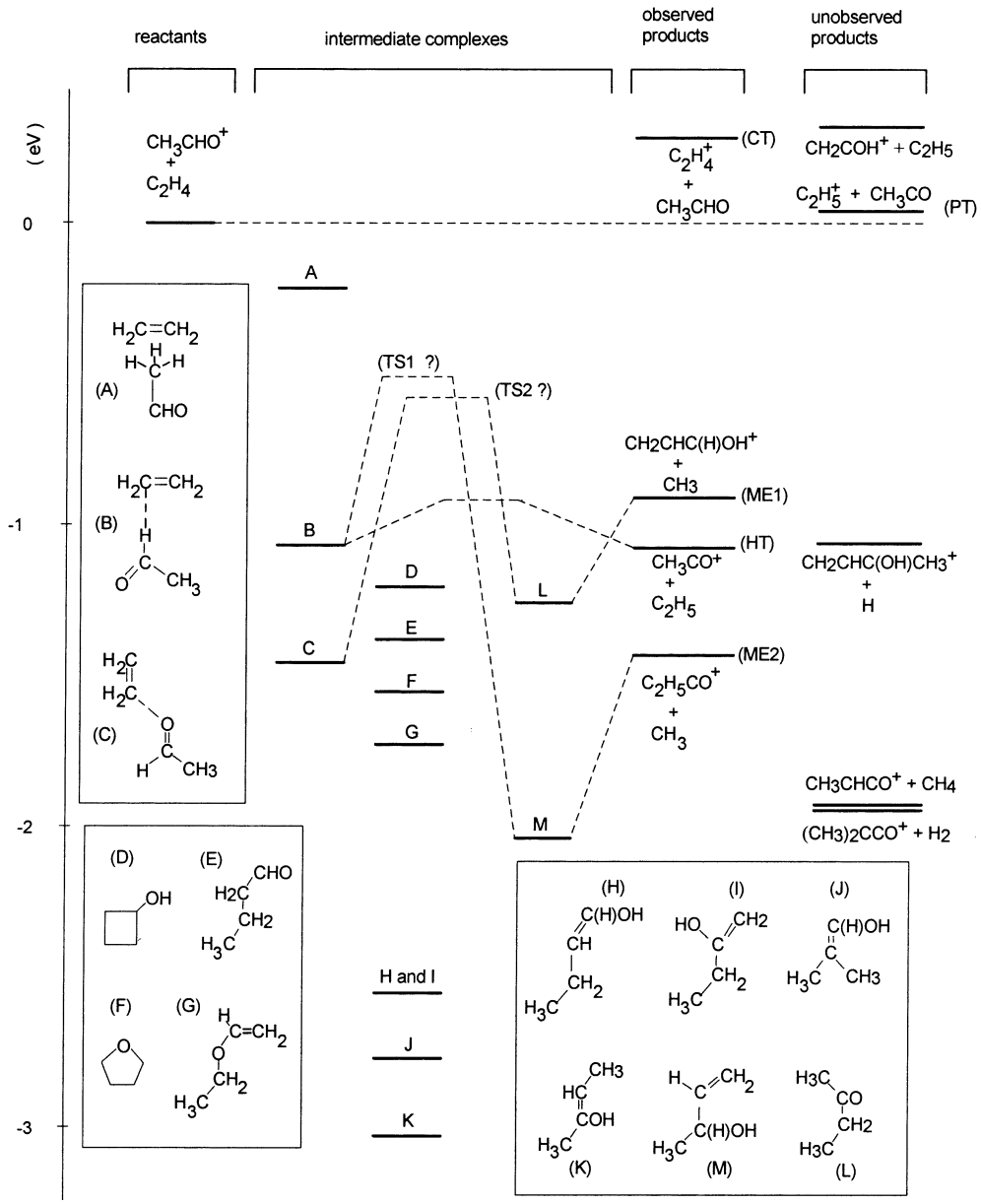

Figure 1. Reaction coordinate diagram showing energetics of reactants, products, and intermediates.

neither isomers nor isotopomers (i.e., structures with the same connectivity and number of D atoms but with different D atom positions). In the discussion that follows, therefore, we will indicate the presence of deuterium labels only in cases where they convey mechanistic information. In Figure 1 and in most locations in the text, we use generic all-H structures. For the CT reaction, only one low-energy product isomer exists, and there is no possibility of isotopomers. For the HT channel, only one low-energy isomer exists, but the ethyl radical product may have two isotopomers. For the ME channel, there are two possible isomeric structures (CH_2═CH═$CHOH^+$ and C_2H_5-CO^+), and each may have isotopomers. Although our experiments cannot distinguish between these isomers, we can say that there is no D-substitution in the eliminated methyl radical (i.e., it appears that it is the intact acetaldehyde methyl group that is being eliminated).

Also shown in Figure 2 is an estimate of the collision cross section taken as the greater value of the capture cross section ($\sigma_{capture}$) or the hard sphere cross section ($\sigma_{hard\ sphere}$). The capture cross section is estimated using the statistical adiabatic channel model of Troe,[14] and the hard sphere cross section (~36 Å^2) is estimated by averaging over different orientations of CH_3CHO^+ and C_2D_4.

The dominant reaction channel at low E_{col} is hydrogen transfer (i.e., production of CH_3CO^+). The ratio of the cross section for methyl elimination to that for hydrogen transfer is just ~0.6% at low E_{col}, even though the methyl elimination channel is more energetically favorable. Methyl elimination is negligible for $E_{collision}$ values above ~0.5 eV. The HT reaction efficiency (shown by the heavy dashed line in Figure 2) can be defined as the ratio of the experimental HT cross section to the collision cross section. For ground-state CH_3CHO^+, $\sigma_{HT}/\sigma_{collision}$ is >73% at low E_{col} and declines to ~24% at E_{col} = 1.95 eV. The cross section for CT rises as E_{col} increases above the endoergicity (0.28 eV) and then becomes energy-independent and roughly equal to σ_{HT} at high E_{col}. Note that the apparent threshold for CT is slightly below the thermodynamic threshold at 0.28 eV, which is a consequence of the distribution of E_{col} resulting from primary ion and target velocity distributions.

Velocity Distributions. Time-of-flight (TOF) is used to record axial velocity distributions for reactant and product ions, as described in detail elsewhere.[1] Axial velocity distributions

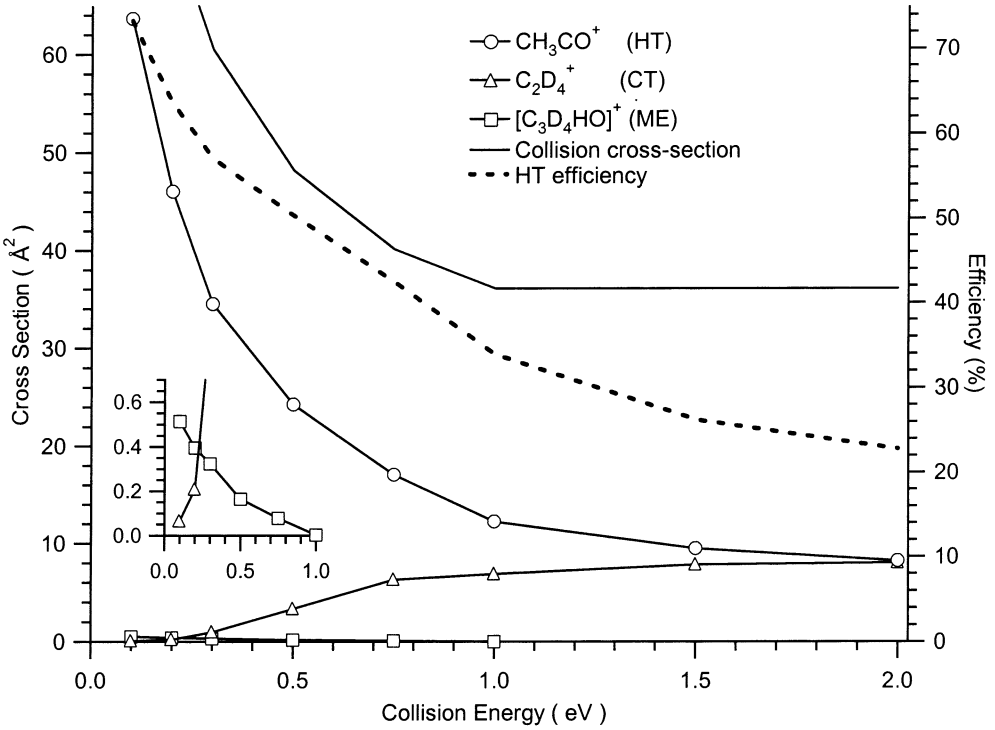

Figure 2. Cross sections for all observed product channels from the reaction of ground-state CH_3CHO^+ and the calculated collision cross section (left-hand scale). Hydrogen transfer (HT) reaction efficiency (right-hand scale). The inset shows an expanded view of the charge transfer (CT) and methyl elimination (ME) channels at low collision energies.

are simply the projection of the full velocity distribution on the ion guide axis. The distributions for the HT, ME, and CT channels are given in Figures 3−5, respectively, and are plotted as laboratory frame velocities. In our experimental geometry, the ion guide is coaxial with the average relative velocity of collisions and with the average velocity of the center-of-mass (V_{CM}). Because of this high symmetry, the axial distributions reveal much of the dynamical information that is contained in the full velocity distributions. For example, the measured laboratory frame distributions can be approximately converted to the center-of-mass frame by simply shifting the origin to V_{CM}, denoted in each frame as a solid vertical line. If the reaction proceeds via a complex with a lifetime ($\tau_{complex}$) that is long compared to its rotational period ($\tau_{rotation}$, typically a few picoseconds), then the recoil velocity distribution must be isotropic in the CM-frame scattering plane of that collision. The resulting axial velocity distribution must be symmetric about V_{CM}. Conversely, a nonsymmetric axial velocity distribution is a clear sign of a fast collision time scale and also reveals the predominant scattering mechanism (e.g., stripping vs rebounding). Finally, the displacement of the v_{axial} peak from V_{CM} provides some information regarding the recoil energies.

Distributions are shown for the reaction of ground-state CH_3CHO^+. For the exoergic ME and HT reactions, the distributions are not significantly different for the reaction of vibrationally excited reactants. An absence of significant vibrational effects on recoil velocity is typical for exoergic reactions of polyatomic ions,[1,15−23] and the reasons for the absence have been discussed recently.[24] The effects of vibration on the endoergic CT channel are discussed below.

The HT velocity distributions (Figure 3) illustrate a problem. Note that at velocities below ∼500 m/sec the distributions are truncated. The TOF for these very slow ions ($E_{LAB} \leq 50$ meV) is easily distorted by potential inhomogeneities in the ion guide, and we are confident of the measured velocity distributions only for higher velocities. The velocity distributions are clearly forward-peaked (ion velocity > V_{CM}) at high collision energies, indicating that the HT process does not involve a long-lived complex. As the collision energy is reduced, V_{CM} decreases, and the peak of the product velocity distribution moves closer to V_{CM}. At $E_{col} = 0.23$ eV, the distribution is still clearly ahead of V_{CM} but only slightly. At $E_{col} = 0.16$ eV, the distribution appears to peak at V_{CM}, but it is not possible to say whether the distribution is symmetric because the entire backward hemisphere is in the low-velocity range where distortions occur. We can conclude that collision time scale for HT is shorter than the complex rotational period for collision energies above 0.23 eV but may be approaching the rotational period at lower energies.

In contrast, the velocity distributions for the ME channel (Figure 4) are forward−backward symmetric even at the highest energies, suggesting that a complex is required to mediate the relatively complicated rearrangements needed to generate stable ME products. The narrow width of the ME v_{axial} distributions (i.e., low recoil velocities) indicates that little of the considerable available energy appears in recoil, which is also consistent with a complex-mediated mechanism.

The most interesting velocity distributions are those for CT. At low energies, the distributions are clearly forward-peaked, indicating rebound scattering (forward = product ions with velocities greater than V_{CM}). Rebound scattering, in turn, suggests that CT is dominated by collisions at small impact parameters b. At high E_{col} values, the distributions become increasingly backward-peaked but with a tail extending into the forward direction. Backward peaking of the ion product corresponds to small-angle scattering, suggesting dominance by collisions at large b. CT is presumably possible in these collisions because E_{col} so greatly exceeds the endoergicity (0.28 eV) that efficient energy conversion is not required. The forward-scattered tail corresponds to CT in low b collisions, but the large b collisions dominate mainly because the probability of collision at a particular b is proportional to b.

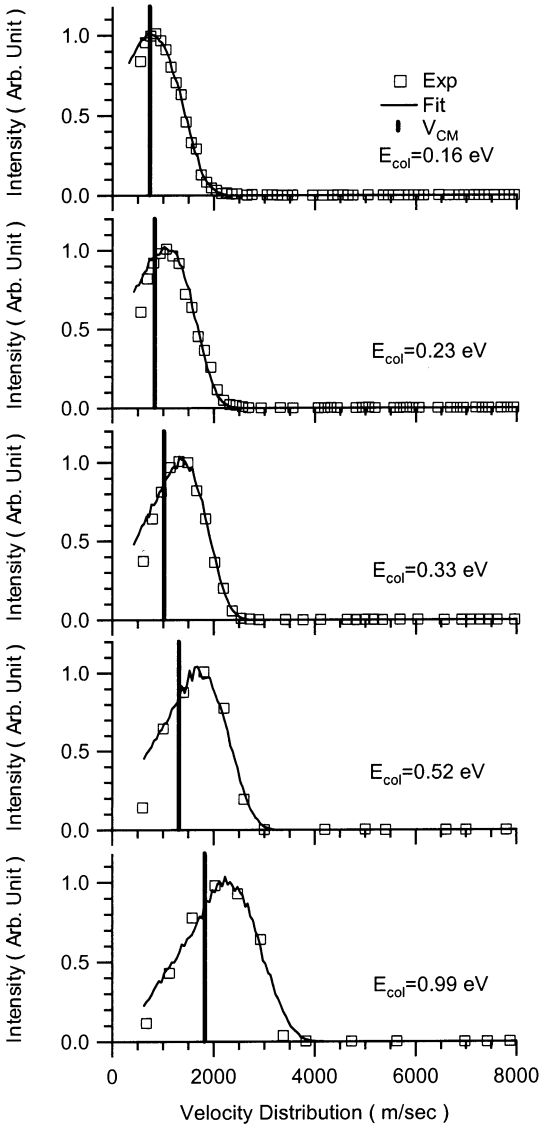

Figure 3. Axial recoil velocity distributions for the hydrogen-transfer ion product from the reaction of ground-state CH_3CHO^+ for several collision energies. The heavy vertical line indicates V_{CM}, the velocity of the center of mass in the lab frame.

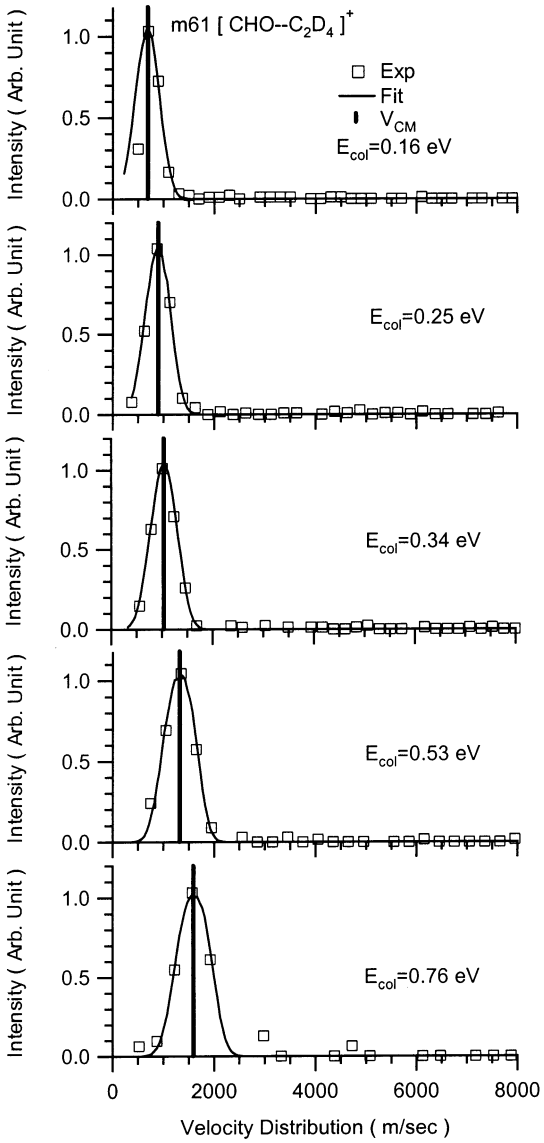

Figure 4. Axial recoil velocity distributions for the methyl elimination ion product from the reaction of ground-state CH_3CHO^+ for several collision energies. The heavy vertical line indicates V_{CM}, the velocity of the center of mass in the lab frame.

We have fit the axial velocity distributions using two different models, and the fits are shown as solid curves through the data points in Figures 3−5. Fitting parameters and results are summarized in Table 2. Fitting allows us to extract quantitative but model-dependent information from the distributions, thus accounting for experimental broadening resulting from the angular and velocity distributions of both reactants. Fitting is done using a Monte Carlo simulation of the experiment described previously.[1]

For the HT reaction, the velocity distributions at our lowest collision energies are forward−backward symmetric, or nearly so, and the energy appearing in recoil (i.e., the width of the distributions) is small despite the considerable exoergicity. As the collision energy is raised, the distributions become asymmetric and broaden faster than would be expected from the increase in the total available energy ($E_{avail} \approx E_{col} + \Delta H_{rxn}$). At the highest energy, the maximum axial recoil velocities are close to the value that would be expected from spectator stripping (SS) dynamics[25,26] (lab frame $v_{SS} = 3890$ m/s), as is often the case for simple atom-transfer reactions.[1,21−23] These results suggest that HT is mediated by a short-lived complex at low collision energies, allowing the available energy to be redistributed among the 33 degrees of freedom. With increasing energy, HT becomes increasingly direct, approaching stripping dynamics at high energies.

The osculating complex model of Fisk et al.[27] was developed to simulate recoil angular distributions for just this sort of reaction in the transition regime between complex-mediated and direct mechanisms. In this model, a complex with a lifetime $\tau_{complex}$ is assumed to form and unimolecularly decompose to products. Within this model, the recoil angular distribution (and thus, the degree of forward−backward asymmetry in the axial distributions) depends only on the ratio of $\tau_{complex}$ to $\tau_{rotation}$, the classical rotational period of the osculating complex. If $\tau_{complex} > \tau_{rotation}$, then the axial velocity distribution must be forward−backward symmetric, but as $\tau_{complex}$ drops below $\tau_{rotation}$, the distributions become increasingly peaked (in this case, in the forward direction). To complete the model, we must assume a recoil energy distribution, $P(E_{recoil})$, that is primarily sensitive to the deviation of the measured distributions from V_{CM}. For simplicity, $P(E_{recoil})$ is assumed to be a Gaussian with adjustable peak and width parameters.[1] Fits were also attempted with the impact parameter model (see below). That model does

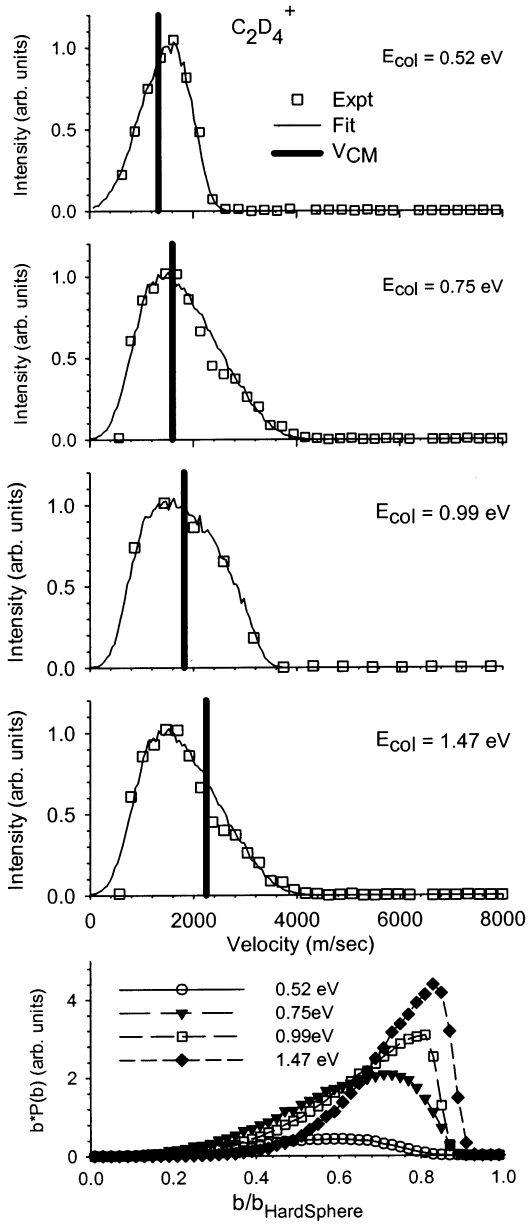

Figure 5. Axial recoil velocity distributions for the charge-transfer ion product from the reaction of ground-state CH_3CHO^+ for several collision energies (top four frames). The heavy vertical line indicates V_{CM}, the velocity of the center of mass in the lab frame. Opacity functions at the indicated collision energies (bottom frame).

not yield sensible fits (i.e., it can fit the data only if HT is assumed to occur only for the narrow range of impact parameters that give strongly sideways-scattered products). Such a restriction is incompatible with the observed large magnitude of the HT cross section, except perhaps at the highest collision energies.

The HT fitting suggests the following: HT collision time scales vary from about 1 ps at low energies to 300 fs at $E_{col} = 1.5$ eV. Over the same E_{col} range, $\langle E_{recoil}\rangle/\langle E_{avail}\rangle$ varies from ~20% to ~30%. Note that for other acetaldehyde cation reactions where the mechanism clearly involves a long-lived complex[15,16,24] (cf. the ME channel in this system), the $\langle E_{recoil}\rangle/\langle E_{avail}\rangle$ ratio is found to be <10% at low collision energies, reflecting extensive energy redistribution in the complex. The fact that the extracted $\langle E_{recoil}\rangle/\langle E_{avail}\rangle$ ratio for HT is more than 20%, even at the lowest energy, is consistent with a short collision time, as is the fact that the distribution is clearly asymmetric even at $E_{col} = 0.23$ eV. For reference, the last column in Table 2 gives the "direct" collision time, which is taken as the time required for 5 Å of relative motion at the speed of the reactants. Note that the collision times extracted from the osculating complex fits are only about a factor of 2 longer than the direct collision times.

TABLE 2: Product Velocity Distribution Fit Results

channel	E_{col} (eV)	$\langle E_{recoil}\rangle$ (eV)	$\langle E_{recoil}\rangle/\langle E_{avail}\rangle$ (%)	$\tau_{complex}$ (ps)	τ_{direct}[c] (ps)
HT	0.16	0.27	20.9	~1[a]	0.4
	0.23	0.30	22.5	0.8	0.33
	0.33	0.33	22.6	0.5	0.27
	0.52	0.42	25.8	0.4	0.22
	0.99	0.57	26.9	0.4	0.16
	1.46	0.72	27.7	0.3	0.13
ME	0.16	0.13	8	>3.4	0.4
	0.25	0.17	10	>3.2	0.33
	0.34	0.19	10	>3.0	0.27
	0.53	0.26	13	>2.6	0.22
	0.76	0.33	14	>2.4	0.18
CT	0.52	0.36	89	−[b]	0.22
	0.75	0.56	92	−	0.18
	0.98	0.78	93	−	0.16
	1.47	1.26	95	−	0.13

[a] $\tau_{complex}$ not well defined for lowest-energy HT distribution because backward hemisphere is outside accessible velocity range. [b] Ocsulating complex model inappropriate and not used in fitting. [c] Direct collision time defined as time for undeflected reactants to travel a relative distance of 5 Å.

For ME, the velocity distributions are symmetric about V_{CM} and are narrow (indicating low recoil energy); both of these characteristics suggest a complex-mediated mechanism. In addition, the nature of the ME reaction almost requires a complex. This channel was also fit using the osculating complex model; however, because the distributions are always symmetric, no information about $\tau_{complex}$ is extracted other than the fact that $\tau_{complex} > \tau_{rotation}$ (Table 2). The main information extracted from the fits to the ME data is the average recoil energy, $\langle E_{recoil}\rangle$, which is tabulated in Table 2 along with the average fraction of the available energy appearing as recoil, $\langle E_{recoil}\rangle/\langle E_{avail}\rangle$. As expected for a mechanism mediated by a complex, $\langle E_{recoil}\rangle/\langle E_{avail}\rangle$ is low, increasing slowly with increasing collision energy.

The osculating complex model is clearly inappropriate for the CT reaction. Even at the lowest energies, CT is direct, and the angular distributions must depend on the range of impact parameters b leading to CT rather than on the rotation of an intermediate complex. In particular, it would be difficult to rationalize the rebound scattering observed at low energies unless CT is restricted to small b. For a similar situation, we developed[15] a simple "impact parameter" model combining energy partitioning based on the line-of-centers model[28] with hard-sphere scattering. For each impact parameter, the collision energy is partitioned into energy along the line-of-centers ($E_{LOC} = E_{collsion}(1 - b^2/d^2)$), and the rest of the energy, E_{rest}. E_{rest} is assumed to remain in translation throughout the collision. E_{LOC} is added to the vibrational energy of the cation (if any) and the rotational energy of the target to give E_{react}, the energy assumed to be available to drive the reaction. If E_{react} is less than the endoergicity, the collision is assumed to be nonreactive. This constraint establishes a maximum reactive impact parameter (b_{cutoff}^{Loc}) for each collision energy, as in the line-of-centers model. For reactive collisions, the recoil energy is assumed to be $E_{recoil} = E_{rest} + (E_{react} - \text{endoergicity})/N_{deg}$, where N_{deg} is the effective number of the degrees of freedom involved in energy partitioning. E_{recoil} is thus the sum of the collision energy

TABLE 3: Experimental and Ab Initio Calculated Energies Relative to Energy of Reactants ($CH_3CHO^+ + C_2H_4$)

reaction energetics (eV)	mp2/6-311++G**	mp2/6-31G*	b3lyp/6-311++G**	b3lyp/6-31G*	G3 (0 K)	exptl
$C_2H_4^+ + CH_3CHO$	−0.11	−0.21	0.18	0.16	0.29	0.28
$C_2H_5^+ + CH_3CO$	−0.13	−0.16	0.22	0.31	0.19	0.03
$CH_2CHCHOH^+ + CH_3$	−0.87	−0.85	−0.52	−0.45	−0.59	−0.91
$C_2H_5 + CH_3CO^+$	−1.57	−1.55	−1.50	−1.58	−1.01	−1.08
$C_2H_5CO^+ + CH_3$	−1.76	−1.74	−0.94	−0.93	−1.20	−1.43
complex A		−0.03	−0.96	−0.85	−0.22	no record
complex B		−1.65	−1.04	−1.14	−1.07	no record
complex C		−1.88	−1.31	−1.52	−1.46	no record
complex D		−1.83	−1.28	−1.19	−1.51	−1.21
complex E		−1.37	−1.22	−1.42	−1.25	−1.38
complex F		−1.66	−1.27	−1.58	−1.38	−1.55
complex G		−2.28	−1.74	−1.99	−1.86	−1.73
complex H		−2.49	−2.10	−2.17	−2.17	−2.55
complex I		−2.65	−2.16	−2.25	−2.34	−2.55
complex J		−2.97	−2.59	−2.66	−2.65	−2.77
complex K		−2.95	−2.56	−2.64	−2.66	−3.03
complex L		−1.35	−0.99	−1.06	−1.09	−1.25
complex M		−2.07	−1.85	−2.06	−1.94	−2.03

not along the line-of-centers plus some fraction of the remaining available energy.

For simplicity, it is also assumed that the impact parameter maps to a unique scattering angle. In our original implementation of this impact parameter fitting model, the angle was taken as the hard sphere deflection angle. Recently, we have obtained more detailed data including full radial and axial velocity distributions for the scattering of formaldehyde from Ne and Xe.[29] That data indicates that the hard sphere angle exceeds the true scattering angle in large impact parameter collisions. Muntean and Armentrout[30] recently proposed an impact parameter/angle mapping function that is based on the conservation of the component of linear momentum perpendicular to the line of centers. With minor modifications, this angular scattering model function also fits our formaldehyde data, and we have adopted it here as well. The present axial velocity fitting is not strongly dependent on the impact parameter/angle mapping function.

With the scattering dynamics defined as just described, the only adjustable inputs to the impact parameter model are the opacity function, $P(b)$, describing the probability of reaction for each impact parameter (constrained by the shape of the distributions) and N_{deg} (constrained by the high-velocity limit of each distribution). In keeping with the attempt to minimize the number of fitting parameters, only very simple opacity functions were used. Fits were first attempted assuming $P(b)$ = constant for $0 < b < b_{cutoff}^{Loc}$ as in the line-of-centers model (where the constant is assumed to be unity). This "no adjustable parameters" model failed to give acceptable fits, with too much intensity for the forward-scattered ions (i.e., small impact parameter collisions). A modified version with constant $P(b)$ values for $b_{min} < b < b_{max}$, where b_{min} and b_{max} ($< b_{cutoff}^{Loc}$) were freely adjustable parameters, also failed. The fits shown were obtained using $P(b)$ in the form of a Gaussian that was truncated at b_{cutoff}^{LOC}. The N_{deg} parameter controls the fraction of the available energy appearing in recoil and is constrained in the fits by the maximum CM recoil velocity (maximum deviation of v_{recoil} from V_{CM}). The best-fit N_{deg} values varied only slightly with E_{col}, from 1.3 at low energy to 1.2 at $E_{col} = 1.47$ eV, corresponding to a situation where most of the available energy is partitioned to recoil, as shown in Table 2. Note that whereas the details of the extracted energy partitioning are highly model-dependent, it is clear from the raw data that a significant fraction of CT reactions does result in high recoil energy.

The impact parameter model fits are shown as curves through the data in Figure 5, and the corresponding opacity functions are given as the product of $bP(b)$ in the fifth frame of the Figure. The $bP(b)$ product is shown because it represents the contribution of each b to the total CT signal. The opacity functions have been scaled so that $\int bP(b)\, db$ is equal to the measured CT integral cross section (Figure 2) at each energy. For low collision energies, the fitting suggests that CT occurs primarily in collisions with impact parameters between ~0.3 and 0.7 of $b_{hardsphere}$, with large b collisions suppressed by the line-of-centers cutoff ($b_{cutoff} \approx 0.7 b_{hardsphere}$) and small b collisions that are simply infrequent. As the collision energy is raised, CT is increasingly dominated by large b collisions, leading to backward-peaked product ions. Such a shift to larger b is not surprising. At high energies, only a small fraction of the collision energy need be converted to drive the endoergic CT process, presumably requiring fewer central collisions. Note that in addition to the increase in average b contributing to CT the magnitude of $P(b)$ increases substantially, indicating that CT probability increases with E_{col} even for small b collisions.

Ab Initio Results. The ab initio results are summarized in Figure 1 and Table 3. For those species where literature energetics are available, the G3 0 K energies are generally in closest agreement, although the discrepancies are frequently more than 0.2 eV. The values used in Figure 1 are experimental (where available) and G3 otherwise. Several complexes with reactant-like geometries were found that were bound by 0.2−1.5 eV with respect to the reactants (A−C in Figure 1). The important geometric parameters for these complexes are summarized in Table 4. As expected for the reaction of an unsaturated molecule, we also find numerous covalently bound complexes (D−M, Figure 1) bound by 1.2−3.0 eV relative to the reactants. Note, however, that the experimental results suggest that these covalent geometries are accessed in at most a small fraction of collisions.

IV. Discussion

The reaction of the acetaldehyde cation with acetylene[16] provides a useful point of comparison for the present reaction with C_2D_4. In both systems, there are many covalently and noncovalently bound complexes, and reaction is dominated by an exoergic HT reaction, with HT efficiency dropping from ~65−75% at low energies to <30% at $E_{col} = 2$ eV. In both systems, the most exoergic channel is ME; however, ME is inefficient, disappearing completely for energies above ~1 eV. The major difference is that CT is not observed for acetylene, presumably because the CT endoergicity is 0.9 eV greater.

TABLE 4: Selected Distances and Angles of Reactant-like Complexes as Results of Ab Initio Calculations[a]

complex A		complex B		complex C	
(D) C1−C	3.457	(D) C1-h	1.746	(D) C1-o	1.603
(D) C2−C	3.470	(D) C1−C2	1.369	(D) C1−C2	1.456
(D) C1−C2	1.364	(D) c−h	1.211	(D) c−o	1.247
(D) C−c	1.530	(D) c−o	1.177	(D) C−c	1.462
(A) C1-c−C2	22.7	(A) C2−C1-h	96.7	(A) C2−C1-o	108.3
(A) C−C1−C2	79.2	(A) C1-h−c	163.5	(A) C1-o−c	121.6
(A) c−C−H	106.7	(A) h−c-o	116.0	(A) o−c-C	121.3
(T) o−c-C1−C2	−121.2	(T) C−c-C1−C2	0.7	(T) c−o-C1−C2	119.6

[a] D = distance (Å), A = angle (deg) ,and T = torsion angle (deg). c, h, and o refer to CHO atoms of the CHO moiety in CH_3CHO^+. C and H refer to CH atoms of the CH_3 moiety in CH_3CHO^+. C1 and C2 refer to C atoms of C_2H_4.

Because the CT channel shows the most interesting dynamics, the discussion will focus there following brief discussions of the HT and ME channels.

Hydrogen Transfer. As Figure 1 indicates, there are many complexes that could serve as intermediates in the reaction of CH_3CHO^+ with C_2D_4. The transition states for interconversion between complexes are unknown; however, given the large amount of energy available in collisional preparation, interconversion is clearly possible. Several observations suggest, however, that most complexes are not accessed in most collisions. Consider the "unobserved products" indicated in Figure 1. A major decomposition pathway for complex K, the most stable complex in our calculations, would almost certainly be through H loss to generate $CH_2CHC(OH)CH_3^+$. The absence of this product channel indicates that complex K is not formed in $CH_3CHO^+ + C_2H_4$ collisions, presumably because the required rearrangements do not compete effectively with the more facile mechanism(s) leading to HT and other product channels. The observation that the HT and CT recoil velocity distributions are asymmetric, except perhaps for HT at our lowest energy, indicates that the collision time scale is short. Similar arguments regarding the H_2-elimination channel would suggest that complex J is not collisionally accessible; however, in this case (and for CH_4 elimination), it is possible that product formation is inhibited by a barrier in the exit channel.

Of perhaps greater overall significance is the fact that none of the observed product ion masses suggests a significant tendency for H/D exchange (i.e., ME always involves CH_3 loss), no CH_3CDO^+ is observed in the "nonreactive" scattering, and there is no $C_2D_3H^+$ product. The absence of H/D exchange suggests that collisions do not access any of the covalently bound complexes D−K, as multiple H-transfer steps must occur in the course of forming and decomposing such intermediates to products, and significant H/D scrambling would be expected.

Given the above information, the likely HT mechanism involves interaction within a geometry similar to that of the hydrogen-bonded complex B, with rapid transfer of the aldehyde H atom and separation to products. Note that in the context of the relatively short time scale HT collisions we refer to the complexes mostly as shorthand for collision geometries, although as shown in Table 2, the collision times extracted from the fits ($\tau_{complex}$) are significantly longer than the times expected for purely direct scattering at low collision energies.

In other systems we have studied, for example, $PhOH^+ + ND_3$[19,20] and $CH_3CHO^+ + D_2O$,[15] substantial H/D exchange is observed in hydrogen-bonded complexes. There are differences between the systems that account for the absence of H/D exchange in complex B for $CH_3CHO^+ + C_2D_4$. In $PhOH^+-ND_3$ and $CH_3CHO^+-D_2O$, the structure of the hydrogen-bonded complexes has the proton transferred (i.e., $PhO-HND_3^+$ and $CH_3CO-HD_2O^+$). Furthermore, both HT and proton transfer product channels are endoergic, so the complex lifetimes are long and the proton is usually transferred back prior to complex breakup. In those complexes, therefore, H/D exchange can occur by a simple rotation of the ND_3H^+ or D_2HO^+ moieties. For $CH_3CHO^+-C_2D_4$, because the exoergic HT reaction is facile, the lifetime of complex B is too short to allow H/D exchange.

The observation that the HT efficiency at low E_{col} (>70%) is substantially larger than the fraction of collisions expected to have the ideal complex B-like geometry indicates that there is some chance for reactant reorientation. As described in detail elsewhere,[16] this effect cannot be due to reorientation as the reactants approach because the torques are too small to cause significant rotation during the approach time. Instead, reactants in nonideal geometries must frequently form a complex (e.g., complex A or C) that lives long enough to allow for rearrangement into the complex B-like geometry where aldehyde H transfer can occur. In this reorientation process, the two reactant molecules evidently retain their identities, so H/D exchange does not occur. The need to invoke reorientation would be avoided if collisions in complex A-like geometry lead directly to transfer of a methyl H atom, giving a product ion indistinguishable by mass. The methyl CH bond is ~1.5 eV stronger than the aldehyde CH bond; however, this channel is endoergic and cannot contribute to the large HT signal at low energies.

The low-energy HT mechanism is perhaps best characterized as a direct aldehyde H-transfer but with reactant reorientation possible, which is mediated by a short-lived, interconverting set of reactant-like precursor complexes (A−C). For collisions in the ideal complex B-like geometry, HT is presumed to be efficient. At higher collision energies, reorientation in the precursor complexes is expected to become insignificant, and the efficiency of aldehyde HT should drop substantially. At the same time, the methyl H-transfer channel opens, possibly offsetting the decrease in aldehyde HT. Note that the observed net HT efficiency is ~25% at high energies, suggesting that methyl HT is not highly efficient.

CH_3CHO^+ vibrational excitation is found to have a weak inhibitory effect on the HT cross section that is nearly independent of E_{col}. The effect is proportional to the vibrational energy (i.e., non-mode-specific) and amounts to only a ~10% inhibition even for the highest-energy vibration ($\langle E_{vib}\rangle = 0.44$ eV). For comparison, at our lowest E_{col}, adding 0.44 eV of collisional energy decreases the cross section by a factor of 4. It is particularly interesting that ν_3, which dominates the vibrational motion for the reactants with $\langle E_{vib}\rangle = 0.44$ eV, has such a small effect. This vibration is the aldehyde CH stretch (i.e., a high-energy stretch of the bond being broken in HT). Simple considerations would suggest that this vibration is strongly coupled to the reaction coordinate and therefore might be expected to have a different effect from other vibrational modes.

The small and non-mode-specific effects are consistent, however, with the precursor complex-mediated reaction mech-

anism outlined above. In this mechanism, the HT efficiency at low energies should depend most strongly on three related factors: the probability of trapping into a precursor complex, the time available for reorientation within the precursor, and branching between the decay of the precursor to HT products versus back to reactants. The strong inhibition by collision energy probably is affected by all three factors. Addition of collision energy decreases the capture collision cross section and probably decreases the probability of trapping into the precursor complex as well. Additional energy will also decrease the lifetime of those precursors that do form. Finally, the angular momentum associated with increased collision energy will tend to favor the decay of precursors back to reactants via an orbiting TS rather than by HT, with its presumably more compact transition state. In contrast, when energy is added as vibration, the capture collisional cross section is unaffected, and trapping into the precursor may be inhibited less than by the same amount of energy in E_{col} because less $T-V$ energy conversion is required. The vibrational energy will reduce the precursor lifetime, but because there is no angular momentum associated with the vibrational energy, there is no bias toward decay back to reactants. The net effect is that E_{col} produces a much larger inhibition than does vibration, as observed. It should be noted that at fixed *total* energy, partitioning energy from E_{col} to vibration substantially increases the HT probability.

Methyl Elimination. The ME product ion recoil velocity distribution is forward−backward symmetric at all energies and also indicates that little energy is partitioned into recoil. Both factors suggest that the mechanism for this channel involves longer collision times, which is not surprising in light of the rearrangements needed to generate stable ME products from reactants. From the structure of the stable ME product ions and the fact that there is no D substitution in the ejected methyl group, it appears likely that the methyl group is ejected from structures such as complexes L and M. Because the potential wells for complexes L and M are shallow and the simple bond scission transition states leading to ME products are expected to be loosely bound, the lifetimes of these product-like complexes are short. For example, the RRKM lifetime for complex M was calculated by assuming an orbiting transition state for CH_3 elimination and by neglecting other possible exit channels from the complex (i.e., giving an upper limit). At all collision energies, the lifetime is less than 100 fs. This time scale is too short to account for the observed forward−backward recoil velocity symmetry and is consistent with the absence of H/D exchange. The implication is that the limiting step in the ME reaction is isomerization from reactant-like geometries to complexes L and M, and it is the reactant-like complexes that are responsible for the observed forward−backward recoil symmetry. Given the nature of the isomerization between reactant-like and ME product-like geometries, slow transition rates are not unexpected. In this scenario, the almost negligible efficiency of the ME reaction is attributable to competition from more facile pathways out of the reactant-like complexes (i.e., HT and dissociation back to reactants).

For the ME reaction, the cross section is too small to allow for meaningful measurement of the effects of the reactant vibrational energy on the cross section.

Charge Transfer. The velocity distributions indicate that CT is dominated by a direct mechanism at all collision energies, with a strong dependence on the impact parameter. Note also that the $\langle E_{recoil}\rangle/\langle E_{avail}\rangle$ fraction (Table 2) is high for CT at all energies. This behavior can be attributed to the fact that the endoergic CT channel is in competition with two other channels that are facile and more energetically favorable. One is HT, which occurs with high efficiency in collisions that trap into precursor complexes (at low energies) or that have the correct geometry for direct H transfer (at all energies). The other competing channel is "no reaction" (i.e., elastic or inelastic scattering). Consider a collision that does not trap into a precursor complex. As the reactants approach each other, the intermolecular interaction mixes the $CH_3CHO^+ + C_2D_4$ and $CH_3CHO + C_2D_4^+$ charge states, as shown by the fact that in all the reactant-like complexes the calculated Mulliken charge is distributed over both moieties. In collisions where there is less than 0.28 eV of collisional to internal energy conversion, energy conservation prevents the endoergic CT reaction. On the other hand, if collisions result in a large collisional to internal energy conversion, then the recoil will be slow. In that case, the separation of the CH_3CHO and C_2D_4 moieties is likely to be electronically adiabatic, so the lower-energy charge state (i.e., reactants) is produced. Separation onto the upper charge-state surface (i.e., CT) requires a collisional to internal energy conversion that is large enough to overcome the endoergicity but not so large to slow the recoil.

The collision energy and reactant vibrational-state dependence of the CT cross section must be considered in light of these factors. At low collision energies, CT is suppressed by three factors: the requirement for substantial collisional to internal energy transfer, trapping into precursor complexes (promoting HT), and the fact that recoil is necessarily slow. As indicated by the axial recoil velocity distributions, CT occurs only for small impact parameter collisions, presumably because these are most likely to result in the required energy transfer. Even then, the CT probability is small, as shown by the small magnitude of $bP(b)$ in Figure 5. With increasing collision energy, a smaller fraction of collisional to internal energy conversion is required, thus allowing collisions at larger impact parameters to contribute. In addition, the rapid rise in the CT cross section implies that the magnitude of $P(b)$ also increases substantially (i.e., the efficiency of CT increases at all impact parameters). This increase is attributed to faster recoil at higher collision energies, thus allowing more nonadiabatic behavior as the products separate.

As might be expected for an endoergic reaction, vibrational excitation enhances the CT cross section, as shown in the inset portion of Figure 6 that shows plots of σ_{CT} versus E_{col} in the threshold energy range. Although the enhancement factors (i.e., $\sigma_v/\sigma_{ground\ state}$) can be quite large near threshold, the effect of vibration is considerably smaller than that from equivalent amounts of collision energy. The relative effectiveness of vibrational and collision energy can be described by a very simple scaling, as shown in the main part of Figure 6. Here we plot the CT cross sections for all reactant vibrational states versus $E_{col} + 0.18E_{vib}$. Except possibly right at threshold, the cross sections for all reactant states are superimposable when plotted this way, indicating that vibration has an enhancing effect that is only 18% of that from collision energy. Although it is surprising that the 18% scaling is constant over such a wide range of E_{col} and E_{vib} values, the CT mechanism proposed above is consistent with a scale factor that is considerably less than unity. Adding energy in the form of reactant vibration reduces the collisional to internal energy transfer required to drive CT, resulting in an enhancement. On the other hand, adding vibrational energy is less likely than an equivalent increase in E_{col} to result in fast product recoil, so the enhancement from vibration is smaller than might be expected.

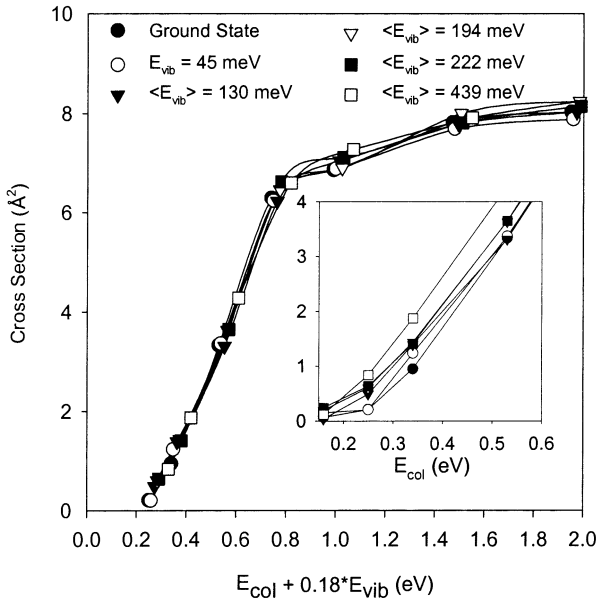

Figure 6. Charge-transfer cross sections plotted vs collision energy plus 18% of the reactant vibrational energy. Charge-transfer cross section as a function of collision energy for six different levels of reactant ion vibrational energy (inset).

For endoergic CT at $E_{col} = 0.52$ eV, the energy available to the products more than doubles when 0.44 eV of vibrational energy is added. One might expect a substantial increase in the recoil energy compared to the energy of the ground-state reactants and a change in the shape of the distribution as well, thereby reflecting changes in the CT dynamics. In fact, there is virtually no effect on the recoil velocity distribution—barely noticeable shifts in peak velocity with no significant changes in width. The shifts are less than the width of the symbols used for data points in Figure 5. Contrast the small effects of vibration with the much larger effects of E_{col}, noting that for $E_{col} = 0.52$ eV and $E_{vib} = 0.44$ eV the total energy is close to that for the ground state at $E_{col} = 0.99$ eV. The fact that the recoil distribution width doesn't change with vibrational excitation implies that energy in reactant vibration tends to remain in product vibration, which is consistent with the relative ineffectiveness of vibration in driving the CT reaction.

Proton Transfer. There is some signal at the proton transfer (PT) product mass ($m/q = 33$) at high E_{col} values ($\sigma_{apparent} = 0.15$ Å^2 at $E_{col} = 1.93$ eV); however, most or all of this signal is attributable to ^{13}C-substituted CT product ions. For example, the mass 33 signal at $E_{col} = 1.93$ eV is ~1.8% of the mass 32 (CT) signal, which is equal to the expected ^{13}C CT signal within experimental uncertainty. The absence of PT is somewhat surprising because PT is generally a highly efficient process, at least in systems where reactions are exoergic with no barriers. In this system, PT is slightly endoergic ($\Delta H = 0.03$ eV), but the available energy greatly exceeds the endoergicity over most of our E_{col} range. Note that the CT reaction has a substantial cross section despite being almost 10 times more endoergic.

We propose that the absence of PT is attributable to competition with the dominant HT channel. These two channels are simply different charge states of the $[CH_3CO + C_2D_4H]^+$ products, with the HT charge state ($CH_3CO^+ + C_2D_4H$) about 1.1 eV lower in energy than the PT charge state ($CH_3CO + C_2D_4H^+$). Although the products are in close proximity, the charge is delocalized over the CH_3CO and C_2D_4H product moieties, as shown by roughly equal calculated Mulliken charges on each moiety in several $CH_3CO-HC_2D_4$ geometries. As the products separate, the system negotiates a series of crossings between vibronic surfaces correlating to HT and PT products. The probability of remaining on the excited electronic surface (i.e., PT) will depend on the relative number of accessible vibronic surfaces associated with the two electronic states as well as on factors relating to the intersurface coupling strengths and crossing velocities.[31] The densities of vibrational−rotational states associated with the two electronic states (at fixed total L and $E = E_{avail}$) should be a reasonable approximation to the number of accessible vibronic surfaces. Because the HT product charge state is substantially lower in energy, the density of states associated with the HT channel is much greater than that associated with PT products. When we also consider that the recoil velocities are relatively slow (favoring adiabatic scattering) it is not surprising that no PT products are observed.

In this regard, the PT−HT competition is much like the competition between CT and "no reaction" discussed above. There, too, density of states and adiabaticity factors tend to suppress the higher-energy charge state. We note that for all the polyatomic ion−molecule reactions we have studied we see CT only in cases where the endoergicity is less than 1 eV.[1,15,16,18−24,32−36] For this system, the CT endoergicity is only 0.28 eV, hence the substantial CT cross section, but the PT−HT energy difference is 1.1 eV.

Acknowledgment. This work was supported by the National Science Foundation under grants CHE-9807625 and CHE-0110318.

References and Notes

(1) Chiu, Y.-H.; Fu, H.; Huang, J.-T.; Anderson, S. L. *J. Chem. Phys.* **1995**, *102*, 1199.
(2) Kim, H.-T.; Anderson, S. L. *J. Chem. Phys.* **2001**, *114*, 3018.
(3) Jochims, H. W.; Lohr, W.; Baumgartel, H. *Chem. Phys. Lett.* **1978**, *54*, 594.
(4) Turecek, F.; Hanus, V. *Org. Mass Spectrom.* **1984**, *19*, 423.
(5) Apeloig, Y.; Karni, M.; Ciommer, B.; Depke, G.; Frenking, G.; Meyn, S.; Schmidt, J.; Schwarz, H. *Int. J. Mass Spectrom. Ion Processes* **1984**, *59*, 21.
(6) Bouma, W. J.; MacLeod, J. K.; Radom, L. *J. Am. Chem. Soc.* **1979**, *101*, 5540.
(7) Bouchoux, G.; Flament, J. P.; Hoppilliard, Y. *Int. J. Mass Spectrom. Ion Processes* **1984**, *57*, 179.
(8) Bertrand, W.; Bouchoux, G. *Rapid Commun. Mass Spectrom.* **1998**, *12*, 1697.
(9) Frisch, M. J.; Trucks, G. W.; Schlegel, H. B.; Scuseria, G. E.; Robb, M. A.; Cheeseman, J. R.; Zakrzewski, V. G.; Montgomery, J. A., Jr.; Stratmann, R. E.; Burant, J. C.; Dapprich, S.; Millam, J. M.; Daniels, A. D.; Kudin, K. N.; Strain, M. C.; Farkas, O.; Tomasi, J.; Barone, V.; Cossi, M.; Cammi, R.; Mennucci, B.; Pomelli, C.; Adamo, C.; Clifford, S.; Ochterski, J.; Petersson, G. A.; Ayala, P. Y.; Cui, Q.; Morokuma, K.; Malick, D. K.; Rabuck, A. D.; Raghavachari, K.; Foresman, J. B.; Cioslowski, J.; Ortiz, J. V.; Stefanov, B. B.; Liu, G.; Liashenko, A.; Piskorz, P.; Komaromi, I.; Gomperts, R.; Martin, R. L.; Fox, D. J.; Keith, T.; Al-Laham, M. A.; Peng, C. Y.; Nanayakkara, A.; Gonzalez, C.; Challacombe, M.; Gill, P. M. W.; Johnson, B. G.; Chen, W.; Wong, M. W.; Andres, J. L.; Head-Gordon, M.; Replogle, E. S.; Pople, J. A. *Gaussian 98*; Gaussian, Inc.: Pittsburgh, PA, 1998.
(10) Foresman, J. B.; Frisch, A. *Exploring Chemistry with Electronic Structure Methods*, 2nd ed.; Gaussian: Pittsburgh, 1993.
(11) Lias, S. G.; Bartmess, J. E.; Liebman, J. F.; Holmes, J. L.; Levin, R. D.; Mallard, W. G. Ion Energetics Data. In *NIST Chemistry WebBook, NIST Standard Reference Database Number 69*; Mallard, W. G., Linstrom, P. J., Eds.; National Institute of Standards and Technology: Gaithersburg, MD (http://webbook.nist.gov), 2000.
(12) Lias, S. G.; Bartmess, J. E.; Liebman, J. F.; Holmes, J. L.; Levin, R. D. *J. Phys. Chem. Ref. Data* **1988**, *17*, suppl. 1.
(13) Zhu, L.; Hase, W. L. *QCPE* 644.
(14) Troe, J. *Chem. Phys. Lett.* **1985**, *122*, 425.
(15) Kim, H.-T.; Liu, J.; Anderson, S. L. *J. Chem. Phys.* **2001**, *115*, 1274.
(16) Kim, H.-T.; Liu, J.; Anderson, S. L. *J. Chem. Phys.* **2001**, *114*, 7838.
(17) Green, R. J.; Anderson, S. L. *Int. Rev. Phys. Chem.* **2001**, *20*, 165.

(18) Kim, H.-T.; Green, R. J.; Anderson, S. L. *J. Chem. Phys.* **2000**, *112*, 10831.
(19) Green, R. J.; Kim, H.-T.; Qian, J.; Anderson, S. L. *J. Chem. Phys.* **2000**, *113*, 4158.
(20) Kim, H.-T.; Green, R. J.; Qian, J.; Anderson, S. L. *J. Chem. Phys.* **2000**, *112*, 5717.
(21) Qian, J.; Green, R. J.; Anderson, S. L. *J. Chem. Phys.* **1998**, *108*, 7173.
(22) Fu, H.; Qian, J.; Green, R. J.; Anderson, S. L. *J. Chem. Phys.* **1998**, *108*, 2395.
(23) Qian, J.; Fu, H.; Anderson, S. L. *J. Phys. Chem.* **1997**, *101*, 6504.
(24) Kim, H.-T.; Liu, J.; Anderson, S. L. *J. Chem. Phys.* **2001**, *115*, 5843.
(25) Henglein, A. L. K.; Jacobs, G. *Ber. Bunsen-Ges. Phys. Chem.* **1965**, *69*, 279.
(26) Henglein, A. L. K. *Adv. Mass Spectrom.* **1966**, *3*, 331.
(27) Fisk, G. A.; McDonald, J. D.; Herschbach, D. R. *Discuss. Faraday Soc.* **1967**, *44*, 228.
(28) Levine, R. D.; Bernstein, R. B. *Molecular Reaction Dynamics and Chemical Reactivity*; Oxford University Press: New York, 1987.
(29) Liu, J.; Van Devener, B.; Anderson, S. L. *J. Chem. Phys.* **2002**, *116*, 5530.
(30) Muntean, F.; Armentrout, P. B. *J. Chem. Phys*. **2001**, *115*, 1213.
(31) Child, M. S. *Molecular Collision Theory*; Academic Press: London, 1974.
(32) Orlando, T. M.; Yang, B.; Anderson, S. L. *J. Chem. Phys.* **1989**, *90*, 1577.
(33) Yang, B.; Chiu, Y. H.; Fu, H.; Anderson, S. L. *J. Chem. Phys.* **1991**, *95*, 3275.
(34) Chiu, Y.-H.; Yang, B.; Fu, H.; Anderson, S. L.; Schweizer, M.; Gerlich, D. *J. Chem. Phys.* **1992**, *96*, 5781.
(35) Chiu, Y.-H.; Fu, H.; Huang, J.-T.; Anderson, S. L. *J. Chem. Phys.* **1996**, *105*, 3089.
(36) Green, R. J.; Kim, H.-T.; Qian, J.; Anderson, S. L. *J. Chem. Phys.* **2000**, *113*, 3002.